MEASUREMENT OF ELASTIC ELECTRON-DEUTERON SCATTERING AT LARGE MOMENTUM TRANSFERS

J. GOMEZ*

Thomas Jefferson National Accelerator Facility
12000 Jefferson Avenue, Newport News, VA 23606, USA
E-mail: gomez@jlab.org

Coincidence measurements of elastic electron-deuteron cross sections have been performed in the range of Q^2 between 0.7 and 6.0 $(\mathrm{GeV/c})^2$. The extracted values of the deuteron electric structure function $[A(Q^2)]$ in this kinematic range are presented. Values of the deuteron magnetic structure function $[B(Q^2)]$ in the range $0.7 \leq Q^2 \leq 1.3\ (\mathrm{GeV/c})^2$ were also extracted and preliminary values are presented. These data are compared with theoretical predictions of both nucleon-meson and quark-gluon based models.

1 Introduction

The unpolarized elastic electron-deuteron cross section is, assuming the exchange of a single virtual photon, given by:

$$\frac{d\sigma}{d\Omega} = \frac{\alpha^2\ E'\ \cos^2\left(\frac{\theta}{2}\right)}{4\ E^3\ \sin^4\left(\frac{\theta}{2}\right)} \left[A(Q^2) + B(Q^2)\ \tan^2\left(\frac{\theta}{2}\right)\right], \tag{1}$$

where α is the fine structure constant, E and E' are the incident and scattered electron energies, θ is the electron scattering angle, and $Q^2 \sim 4EE'\sin^2(\theta/2)$ is the invariant four-momentum transfer. The electric $[A(Q^2)]$ and magnetic $[B(Q^2)]$ deuteron structure functions are given in terms of the charge monopole $[F_c(Q^2)]$, charge quadrupole $[F_q(Q^2)]$, and magnetic dipole $[F_m(Q^2)]$ form factors by:

$$A(Q^2) = F_c^2(Q^2) + \frac{8}{9}\tau^2 F_q^2(Q^2) + \frac{2}{3}\tau F_m^2(Q^2), \tag{2}$$

$$B(Q^2) = \frac{4}{3}\tau(1+\tau)F_m^2(Q^2), \tag{3}$$

where $\tau = Q^2/4M^2$ and M is the deuteron rest mass.

The structure functions $A(Q^2)$ and $B(Q^2)$ can be separated by measuring two or more unpolarized cross section values at a constant value of Q^2 and

*REPRESENTING THE JLAB HALL A COLLABORATION.

different electron scattering angles θ. This method is referred to as the Rosenbluth technique. To separate the individual $F_c(Q^2)$ and $F_q(Q^2)$ contributions, an additional polarization observable is needed.

The experiment being reported here measured unpolarized cross sections in the range of $0.7 \leq Q^2 \leq 6.0$ (GeV/c)^2 and $15.5^\circ \leq \theta \leq 40.6^\circ$ to extract $A(Q^2)$ [forward data]. Cross sections were also measured in the range of $0.7 \leq Q^2 \leq 1.3$ (GeV/c)^2 at a fixed angle of $\theta = 144.5^\circ$ [backward data] which allowed separation of $A(Q^2)$ and $B(Q^2)$ in this Q^2 range via the Rosenbluth technique.

2 Experiment

The experiment was conducted in Hall A at the Thomas Jefferson National Accelerator Facility (JLab). Incident electron beams with a 100% duty factor, energies from 0.5 to 4.4 GeV, and beam currents from 5 to 120 μA were used. Beam current and energy uncertainties were estimated to be $\pm 2\%$ and $\pm 0.2\%$, respectively. Uncertainties due to beam position and angle at the target are negligible.

The target system consisted of three independent loops. Two of the loops were filled with liquid deuterium and the third with liquid hydrogen. Each loop consisted of a 15 cm long cylindrical target cell with its long axis of symmetry parallel to the beam path, a heat exchanger to remove the heat deposited by the beam in the liquid, and a fan system that circulated the liquid between the target cell and the heat exchanger. The heat exchange system maintained the liquid deuterium (hydrogen) at a temperature of 22 (19) K and a pressure of 22 (27) psia.

One of the deuterium targets was used exclusively for the forward-angle measurements while the other was used to acquire all the backward data. The latter target had a collimator attached to it on the electron spectrometer side. The collimator allowed the electron spectrometer to view a well-defined section of the target cell ($\sim$10cm) at 144.5° without interference from angle dependent obstructions due to the target cell design used by this experiment.

In order to reduce beam-induced density changes, the beam was rastered in both the horizontal and vertical direction in a $\sim$2x2 mm^2 pattern at frequencies of 17.6 and 24.4 kHz respectively. Measured beam-induced deuterium density changes were $\sim$2.5% at 120 μA. A 15 cm long "empty" target was used to measure possible contributions from the full cell end-caps to the measured cross sections. They were found to be negligible.

The Hall A experimental facility consists of two identical High Resolution Spectrometers (HRS) of the type QQDQ. The dipole has a built-in index

which provides additional focusing. One of the HRSs was set to bend negatively charged particles into its focal plane (electron HRS) while the other for positive particles (recoil HRS). Each HRS was instrumented with two planes of plastic scintillators for triggering and timing as well as a pair of vertical drift chambers for track reconstruction. In addition, the electron HRS was equipped with a CO_2 gas Čerenkov and a lead-glass calorimeter for electron identification. The trigger logic was set to accept all electron-recoil spectrometer coincidences as well as samples of single-arm triggers for detector efficiency studies.

Coincidence elastic electron-proton (e-p) cross sections were measured in this experiment to check our understanding of spectrometer optics and double-arm acceptance. The e-p kinematics were selected such that the electron-recoil solid angle Jacobian for e-p was the same as for electron-deuteron (e-d) for all forward angle data. For the $\theta = 144.5°$ e-d data, the corresponding e-p data was taken at a fixed angle $\theta = 90°$ to avoid any partial occlusion of the hydrogen target cell. The Jacobian ratio of e-p to e-d was ~ 0.7 for these conditions. All the e-p and the low Q^2 e-d data were taken with and without solid-angle defining collimators in front of the spectrometers. The large Q^2 e-d data was taken without collimators due to the small cross sections measured.

In the data analysis, the electron spectrometer section of a raw coincidence event was first validated by requiring a pulse height in the Čerenkov counter above pedestal and an energy deposition in the calorimeter of at least 60% of the momentum determined from the drift chamber track. Raw coincidence events passing the above cuts were then required to have relative time-of-flight (TOF) between the electron and recoil triggers of $\pm$ 7.5 nanoseconds or less. Random coincidences were negligible.

The elastic e-p and e-d cross sections were calculated according to:

$$\frac{d\sigma}{d\Omega} = \frac{N_{ep(ed)}\ C}{N_i\ N_t\ F\ \Delta\Omega}, \tag{4}$$

where $N_{ep(ed)}$ is the number of e-p (e-d) coincidence events passing the cuts described above, N_i is the number of incident electrons, N_t is the number of target-nuclei/cm^2, $\Delta\Omega$ is the effective double-arm solid angle including the spectrometer-acceptance dependent part of the radiative corrections, F is the portion of the radiative corrections that depends only on Q^2 and target thickness. C is the product of corrections such as detector inefficiency (1%), trigger inefficiency including proton (2.5-2.8%) and deuteron (3.2-3.5%) absorption in the scintillators, computer dead time (typically 10% for e-d), and proton (forward data: 0.7-1.8%, backward data: 0.8%) and deuteron (forward data: 2.8-5.1%, backward data: 5.6-8.2%) absorption in the target and spectrometer

windows.

The effective double-arm solid angle $\Delta\Omega$ was evaluated with a Monte Carlo computer program that simulated elastic *e-p* and *e-d* scattering under identical conditions as our measurements. The program traced scattered electrons and recoil nuclei from the target to the detectors through models representing the magnetic characteristics, physical apertures, and alignment of each HRS. The effects from ionization energy losses and multiple scattering in the target and vacuum windows were taken into account for both electrons and recoil nuclei. Bremsstrahlung radiation losses for both incident and scattered electrons in the target and vacuum windows as well as internal radiative effects were also taken into account. Details on this simulation method can be found in Katramatou *et al.* [1]

The elastic *e-p* cross sections measured with the acceptance-defining collimators were found to agree, on average, within 0.3% with the values calculated from a recent parametrization of the proton electromagnetic form factors by Bosted *et al.* [2] Elastic *e-p* cross sections measured without collimators were found to be higher by 2.6% than the values calculated from the same parametrization. Consequently, the elastic *e-d* cross sections taken without collimator have been normalized by this amount.

3 Results

Values of $A(Q^2)$ were extracted from the measured forward-angle *e-d* cross sections under the assumption that $B(Q^2)$ does not contribute in any sizable way to the cross section (supported by the existing $B(Q^2)$ data). The extracted $A(Q^2)$ values are presented in Fig. 1. The error bars represent statistical and systematic uncertainties added in quadrature. The statistical error ranged from $\pm 1\%$ to $\pm 30\%$ at $Q^2 = 6$ (GeV/c)^2. The systematic error has been estimated to be $\sim \pm 6\%$. Our results agree very well with previous SLAC data and continue to follow the trend of a smooth fall-off versus momentum transfer. Figure 2 shows our preliminary values of $B(Q^2)$. The error bars include statistical and systematic uncertainties added in quadrature and range from 5% at 0.7 (GeV/c)^2 to 20% at 1.3 (GeV/c)^2. Our data agree well with previously existing data but do not reach far enough in momentum transfer to confirm the location of the $B(Q^2)$ minimum observed in the SLAC data.

Results from several theoretical calculations are also shown in Figs. 1 and 2. The predictions by Hummel and Tjon[9] (HT) are shown as curves [a] and [b] in Fig. 1 and [c] in Fig. 2. The HT calculations use the Blankenbecler-Sugar equation,[13] a "quasipotential" approximation of the Bethe-Salpeter

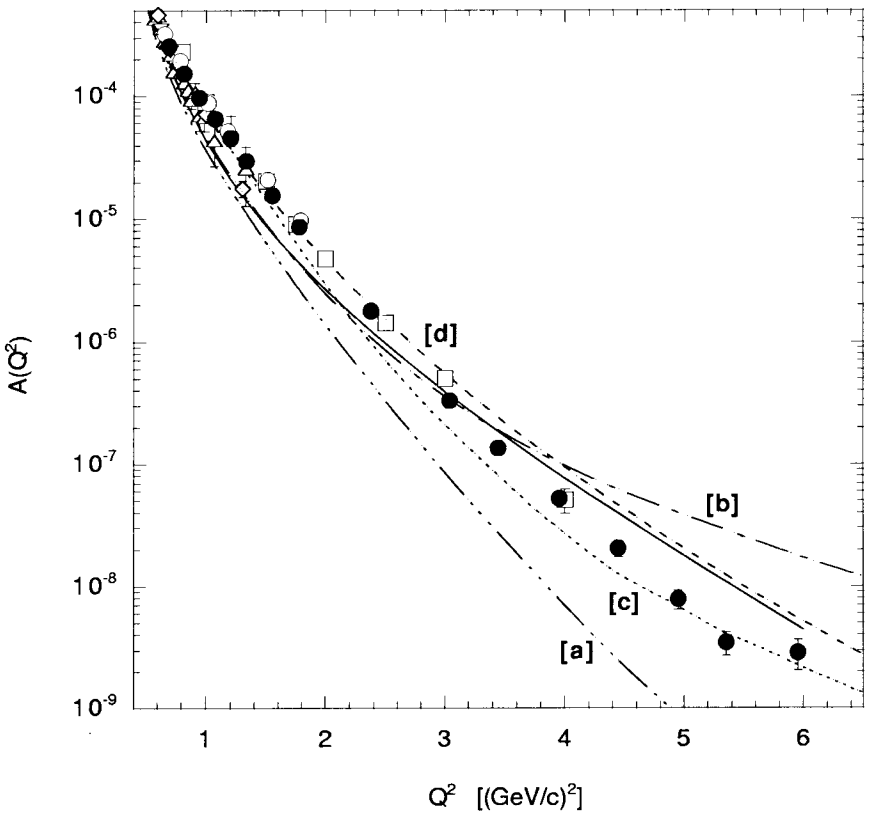

Figure 1. Shown are the values of $A(Q^2)$ obtained by this experiment [3] [•] together with existing data from CEA [4] [△], SLAC [5] [□], Bonn [6] [◇], Saclay [7] [▽] and, JLab-C [8] [○]. Also shown are theoretical predictions from Hummel and Tjon [9] without [a] and with [b] meson exchange currents (MEC), Van Orden *et al.* [10] [c] and Carbonell and Karmanov [14] [d]. The solid line represents the model of Lev *et al.*[15]

(BS) equation[11] obtained by allowing both nucleons to be equally off-shell so that their relative energy is set to zero. The nucleon form factor parametrization of Höhler *et al.*[16] is used. Calculations of $A(Q^2)$ based on the relativistic impulse approximation (RIA) without meson exchange currents (MEC) typically lack enough strength at large Q^2 to account for the data (curve [a] of Fig. 1). Additional strength is obtained by including the effects of MEC and isobar contributions in the calculations. For elastic scattering from the

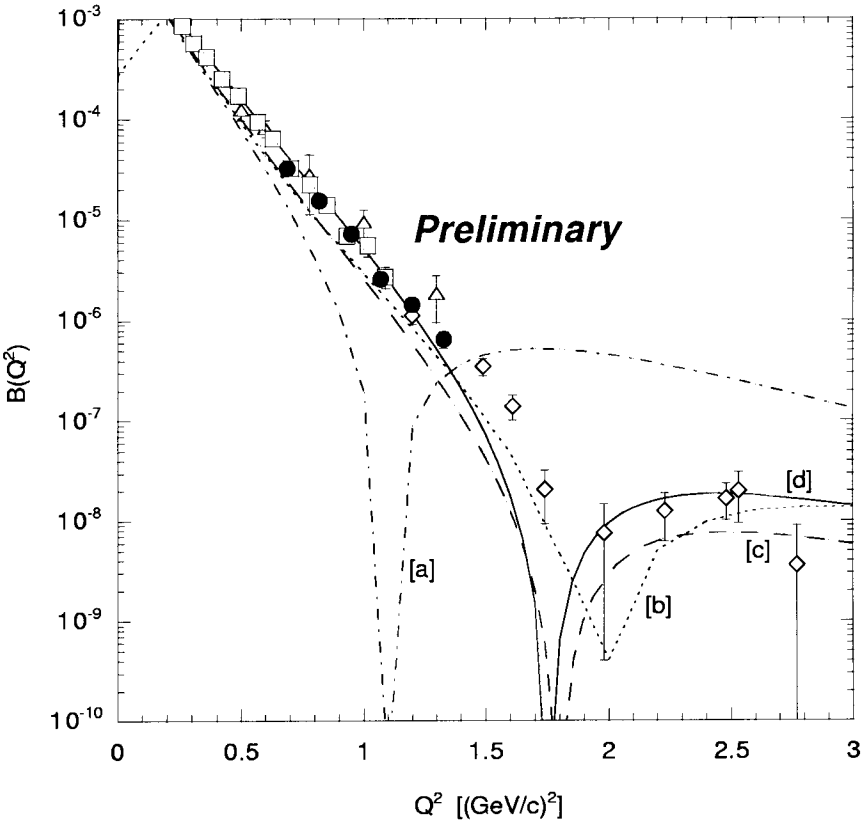

Figure 2. Preliminary values of $B(Q^2)$ obtained by this experiment [•] together with existing data from Bonn[6] [△], Saclay[18] [□] and, SLAC[19] [○]. Also shown are theoretical predictions from Carbonell and Karmanov [14] [a], Lev *et al.* [15] [b], Hummel and Tjon [9] [c] and, Van Orden *et al.* [10] [d].

deuteron, only isoscalar two-body exchange currents such as $\rho\gamma\pi$, $\omega\sigma\gamma$, $\omega\eta\gamma$, etc. contribute. However, the form factors for these exchange currents are neither experimentally known nor theoretically constrained by an invariance. Their behavior needs to be modeled. In the HT case, the $\rho\pi\gamma$ and $\omega\sigma\gamma$ MEC have been included with form factors given by the vector dominance model (VDM) (curve [b] of Fig. 1 and curve [c] of Fig. 2). In this model, the $\rho\pi\gamma$ MEC has a larger effect in $A(Q^2)$ than the $\omega\sigma\gamma$ MEC. The situation is

reversed for $B(Q^2)$.

Curves [c] of Fig. 1 and [d] of Fig. 2 show the predictions of Van Orden *et al.*[10] This model uses the Spectator (or Gross) equation,[12] a "quasipotential" approximation of the BS equation obtained by restricting one of the nucleons to its positive energy mass shell. The model includes a $\rho\pi\gamma$ MEC evaluated in a covariant-separable-quark model[21] which gives a "softer" Q^2 dependence of the $\rho\pi\gamma$ form factor. The location of the $B(Q^2)$ diffraction minimum in the Van Orden *et al.* model is very sensitive to the interference between S and D components of the deuteron wave function with the two smaller P-state components.

The predictions by Carbonell and Karmanov[14] are shown as curves [d] and [a] of Figs. 1 and 2 respectively. The approach taken by these authors uses an explicitly covariant version of the Light-Front Dynamics (LFD) but with a deuteron wavefunction which is calculated perturbatively from the non-relativistic wave function.[22] For the one-boson exchange kernel found in the LFD calculation, the set of mesons, coupling constants, and form factors corresponding to the Bonn model[23] were used. The nucleon form factors used are those of Mergell *et al.*[24] The results of the calculation for $A(Q^2)$ agree well with the data up to $Q^2 \sim 2.5$ (GeV/c)^2 (see Fig. 1). Departure between the experiment and theory for larger Q^2 is attributed to the use of the non-relativistic deuteron wave function. The location of the $B(Q^2)$ diffraction minimum predicted by this model (see Fig. 2) is sensitive to the interference among various components of the deuteron wave function. The authors believe that the perturbative approach used to calculate the deuteron wave function does not provide enough accuracy in the calculation of these components.

The solid line of Fig. 1 and curve [b] of Fig. 2 show the predictions of Lev, Pace, and Salme[15] for $A(Q^2)$ and $B(Q^2)$. The authors use the front-form approach but select the Breit frame to build a current operator (obtained from the free current) which meets all the requirements of extended Poincare covariance. The predictions shown make use of the nucleon form factor parametrization of Höhler *et al.*[16] and the Argonne AV18[17] nucleon-nucleon potential.

Deuteron models based on dimensional scaling[26,27] and perturbative QCD[28] predict the deuteron form factor $F_d(Q^2) \equiv \sqrt{A(Q^2)}$ to fall as $(Q^2)^{-5}$. Consequently, the quantity $A(Q^2) \times (Q^2)^{10}$ should scale. Our data exhibits a scaling behavior compatible with those expectations (top panel of Fig. 3). The bottom panel of Fig. 3 shows the reduced deuteron form factor $f_d(Q^2) \equiv F_d(Q^2)/F_N^2(Q^2/4)$ where the two powers of the nucleon form factor $F_N(Q^2) = (1 + Q^2/0.71)^{-2}$ remove in a minimal way the effects of nucleon structure.[29] Our $f_d(Q^2)$ data appear to follow, for $Q^2 > 2$ (GeV/c)^2, the

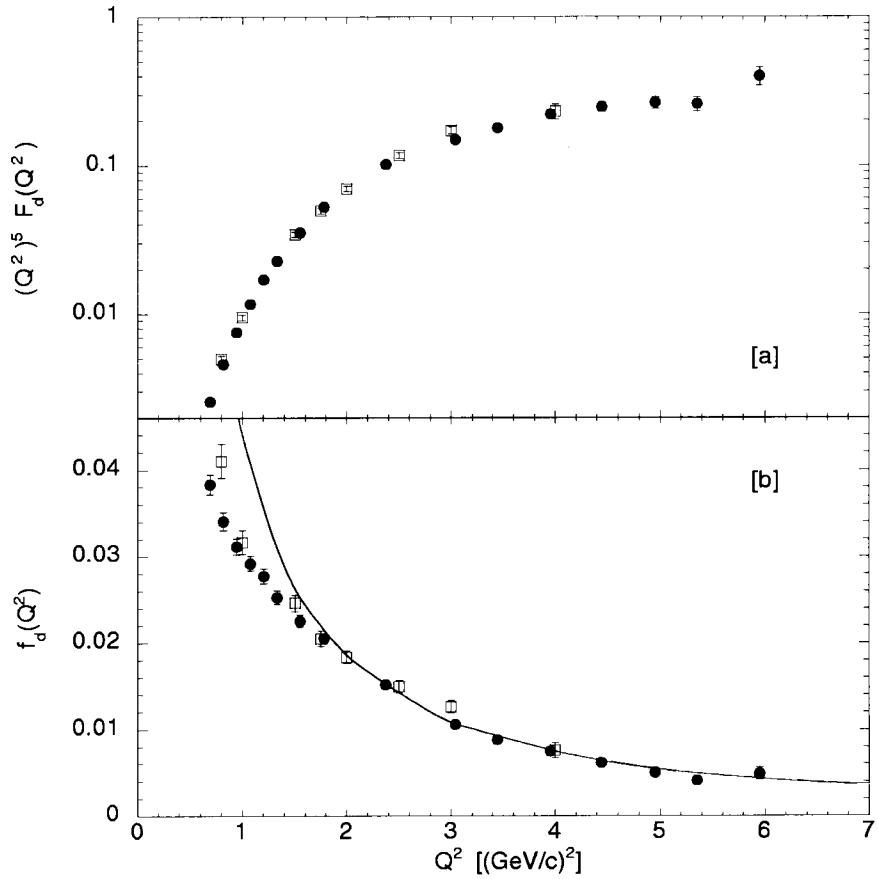

Figure 3. The deuteron form factor $F_d(Q^2)$ times $(Q^2)^5$ [a] and the reduced deuteron form factor $f_d(Q^2)$ [b] from this experiment [•] and from SLAC[5] [□]. The solid curve represents the asymptotic pQCD prediction of Brodsky *et al.*[25] for $\Lambda = 100$ MeV, arbitrarily normalized to the data at $Q^2 = 4$ (GeV/c)^2.

asymptotic Q^2 prediction of pQCD.[25] Although several authors have questioned the validity of dimensional scaling and pQCD at the momentum transfers of this experiment,[30,31] similar scaling-like behavior has been reported in deuteron photodisintegration cross sections at moderate photon energies.[32]

In summary, we have extended the measured range of $A(Q^2)$ up to 6

$(\mathrm{GeV/c})^2$ and clarified inconsistencies in previous low Q^2 data. Our $B(Q^2)$ results confirm previous measurements[19] and improve their precision. The measured $A(Q^2)$ data have a dependence on momentum transfer which is qualitatively reproduced by the conventional nuclear physics models presented above. The results are also consistent with predictions of dimensional quark scaling and perturbative QCD. On the theoretical side, the location of the $B(Q^2)$ diffraction minimum is very sensitive to the details of the model used. It is therefore essential to extend the measurements of $B(Q^2)$ to higher momentum transfers to test the validity of the various models proposed. Future measurements at higher Q^2 of $A(Q^2)$ and $B(Q^2)$ as well as of the elastic form factors of the helium isotopes are also essential to test the validity of the apparent scaling behavior observed.

The outstanding support of the staff of the Accelerator and Physics Divisions of JLab is gratefully acknowledge. The work described in this paper was supported in part by the U.S. Department of Energy and the National Science Foundation.

References

1. A.T. Katramatou *et al.*, Nucl. Instr. Meth. **A267**, 448 (1988).
   A.T. Katramatou, SLAC-NPAS-TN-86-08, 1986 (unpublished).
2. P.E. Bosted *et al.*, Phys. Rev. **C51**, 409 (1995).
3. L.C. Alexa *et al.*, Phys. Rev. Lett. **82**, 1374 (1999).
4. J.E. Elias *et al.*, Phys. Rev. **177** 2075 (1969).
5. R.G. Arnold *et al.*, Phys. Rev. Lett. **35**, 776 (1975).
6. R. Cramer *et al.*, Z. Phys. **C29**, 513 (1985).
7. S. Platchkov *et al.*, Nucl. Phys. **A510**, 740 (1990).
8. D. Abbott *et al.*, Phys. Rev. Lett. **82**, 1379 (1999).
9. E. Hummel and J.A. Tjon, Phys. Rev. Lett. **63**, 1788 (1989).
   E. Hummel and J.A. Tjon, Phys. Rev. **C42**, 423 (1990).
10. J.W. Van Orden, N. Devine, and F. Gross, Phys. Rev. Lett. **75**, 4369 (1995) and references therein.
11. E.E. Salpeter and H.A. Bethe, Phys. Rev. **84**, 1232 (1951).
12. F. Gross, Phys. Rev. **186**, 1448 (1969); Phys. Rev. **D10**, 223 (1974); Phys. Rev. **C26**, 2203 (1982).
13. R. Blankenbecler and R. Sugar, Phys. Rev. **142**, 1051 (1966).
14. J. Carbonell and V.A. Karmanov, Los Alamos preprint nucl-th/9902053.
15. F.M. Lev, E. Pace, and G. Salme, Los Alamos preprint nucl-th/9812030.
16. G. Höhler *et al.*, Nucl. Phys. **B114**, 505 (1975).
17. R.B. Wiringa, V.G.J. Stoks, and R. Schiavilla, Phys. Rev. **C51**, 38

(1995).
18. S. Auffret *et al.*, Phys. Rev. Lett. **54**, 649 (1985).
19. R.G. Arnold *et al.*, Phys. Rev. Lett **58**, 1723 (1987).
P.E. Bosted *et al.*, Phys. Rev. **C42**, 38 (1990).
20. H. Ito and F. Gross, Phys. Rev. Lett. **71**, 2555 (1993).
21. K.L. Mitchell, Ph.D. Dissertation, Kent State University, 1995.
P.C. Tandy, Prog. Part. Nucl. Phys. **36**, 97 (1996).
22. J. Carbonell and V.A. Karmanov, Nucl. Phys. **A581**, 625 (1995).
23. R. Machleidt, K. Holinde, and Ch. Elster, Phys. Reports **149**, 1 (1987).
24. P. Mergell, U-G. Meissner, and D. Drechsell, Nucl. Phys. **A596**, 367 (1996).
25. S.J. Brodsky, C-R. Ji, and G.P. Lepage, Phys. Rev. Lett. **51**, 83 (1983).
26. S.J. Brodsky and G.R. Farrar, Phys. Rev. Lett. **31**, 1153 (1973).
27. V Matveev *et al.*, Nuovo Cimento Lett. **7**, 719 (1973).
28. S.J. Brodsky *et al.*, Phys. Rev. Lett. **51**, 83 (1983).
29. S.J. Brodsky and B.T. Chertok, Phys. Rev. Lett. **37**, 269 (1975).
30. N. Isgur and C.H. Llewellyn Smith, Phys. Rev. Lett. **52**, 1080 (1984); Phys. Lett. **217**, 535 (1989).
31. G.R. Farrar, K. Huleihel, and H. Zhang, Phys. Rev. Lett. **74**, 650 (1995).
32. C. Bochna *et al.*, Phys. Rev. Lett. **81**, 4576 (1998).